EUKARYOTIC CELL, Nov. 2008, p. 1916–1929 Vol. 7, No. 11
1535-9778/08/$08.00+0 doi:10.1128/EC.00237-08

A Signaling-Regulated, Short-Chain Dehydrogenase of *Stagonospora nodorum* Regulates Asexual Development▽‡

Kar-Chun Tan,[1] Joshua L. Heazlewood,[2]† A. Harvey Millar,[2] Gordon Thomson,[3] Richard P. Oliver,[1] and Peter S. Solomon[1]*

Australian Centre for Necrotrophic Fungal Pathogens, SABC, Faculty of Health Sciences, Murdoch University, Murdoch 6150, Australia[1]; Australian Research Council Centre of Excellence in Plant Energy Biology, The University of Western Australia, Crawley 6009, Australia[2]; and School of Biological Sciences and Biotechnology, Division of Science and Engineering, Murdoch University, Murdoch 6150, Australia[3]

Received 17 July 2008/Accepted 22 August 2008

The fungus *Stagonospora nodorum* is a causal agent of leaf and glume blotch disease of wheat. It has been previously shown that inactivation of heterotrimeric G protein signaling in *Stagonospora nodorum* caused development defects and reduced pathogenicity [P. S. Solomon et al., Mol. Plant-Microbe Interact. 17:456–466, 2004]. In this study, we sought to identify targets of the signaling pathway that may have contributed to phenotypic defects of the signaling mutants. A comparative analysis of *Stagonospora nodorum* wild-type and Gα-defective mutant (*gna1*) intracellular proteomes was performed via two-dimensional polyacrylamide gel electrophoresis. Several proteins showed significantly altered abundances when comparing the two strains. One such protein, the short-chain dehydrogenase Sch1, was 18-fold less abundant in the *gna1* strain, implying that it is positively regulated by Gα signaling. Gene expression and transcriptional enhanced green fluorescent protein fusion analyses of *Sch1* indicates strong expression during asexual development. Mutant strains of *Stagonospora nodorum* lacking *Sch1* demonstrated poor growth on minimal media and exhibited a significant reduction in asexual sporulation on all growth media examined. Detailed histological experiments on *sch1* pycnidia revealed that the gene is required for the differentiation of the subparietal layers of asexual pycnidia resulting in a significant reduction in both pycnidiospore size and numbers.

The heterotrimeric G protein family is a universal eukaryotic signaling component. The heterotrimer consists of α, β, and γ subunits that are coupled to the cytoplasmic side of a membrane-bound G protein-coupled receptor. The binding of a ligand to the G protein-coupled receptor causes the exchange of GDP for GTP on the Gα subunit resulting in its dissociation from the Gβ-Gγ complex. The released Gα subunit can then activate downstream cellular effectors (4, 51). Four different classes of mammalian Gα proteins have been proposed based on the amino acid sequence relationships (39). The $G\alpha_s$ and $G\alpha_i$ classes function to stimulate and inhibit cyclic AMP production, respectively, whereas $G\alpha_q$ subunits function within the phosphatidylinositol pathway and $G\alpha_{12/13}$ activates signaling through the small Rho GTPase (27, 39).

The roles of heterotrimeric G proteins in plant pathogenic fungi have been extensively studied (3, 28). At least 23 Gα genes of plant pathogenic fungi have been reported in the literature thus far. These 23 genes can be subdivided into two groups related to the mammalian $G\alpha_s$ and $G\alpha_i$ proteins based on the amino acid sequences (3). Mutants that are impaired in $G\alpha_i$ subunits often possess significant phenotypic defects that can affect the fitness of the pathogen (11, 14, 16, 21, 22, 31, 32, 46, 56, 66), implying that this signal transduction system controls processes vital for pathogenicity (Table 1). Transcriptomics has been used to elucidate targets of $G\alpha_i$ subunit signaling in the gray mold *Botrytis cinerea* and the chestnut blight fungus *Cryphonectria parasitica*. These studies have shown signaling regulation of the botrydial toxin gene *bot1* in *B. cinerea* (17, 50) and hypovirus-responsive genes in *C. parasitica* (8), respectively.

Proteomic approaches provide a complementary means of identifying targets of G protein signaling. Previously, such approaches have been used to study phytopathogenic fungi through protein profiling (2, 5, 12, 42, 44) and to identify host- (45) and morphogenesis-responsive (25) proteins. Recent sequencing of the genomes of the phytopathogenic fungi *Magnaporthe grisea*, *Ustilago maydis*, *Fusarium graminearum*, and *Stagonospora nodorum* (7, 9, 19, 24) provides an opportunity for more thorough mass spectrometry (MS)-based proteomic analyses (2, 42).

Stagonospora nodorum is a major fungal pathogen of wheat (53). The role of signal transduction in the pathogenicity of *S. nodorum* has been recently scrutinized (54, 56, 59). Of particular interest were strains harboring an impaired Gα gene, *Gna1*. Mutants were reduced in their ability to colonize the host, and they failed to sporulate, showed an albino phenotype, and reduced extracellular depolymerase activities. It was hypothesized that these impairments were a result of changes in the state or abundance of heterotrimeric G protein signaling targets. The aim of this experiment was to identify and functionally characterize proteins regulated by the Gna1 protein by using two-dimensional polyacrylamide gel electrophoresis (2D-

* Corresponding author. Mailing address: ACNFP, FHS, Murdoch University, South Street, Murdoch 6150, Australia. Phone: 61 8 9360 7239. Fax: 61 8 9310 4144. E-mail: p.solomon@murdoch.edu.au.

† Present address: Joint Bioenergy Initiative, Lawrence Berkeley Laboratories, CA.

‡ Supplemental material for this article may be found at http://ec.asm.org/.

▽ Published ahead of print on 5 September 2008.

TABLE 1. Phenotypes of plant pathogenic fungi defective in $G\alpha_i$ protein signaling

Organism	$G\alpha_i$ gene	Functions
Stagonospora nodorum	*Gna1*	Pycnidiation, extracellular protease secretion, DOPA metabolism, and virulence
Alternaria alternata	*Aga1*	Conidial germ tube formation and virulence
Botrytis cinerea	*Bcg1*	Vegetative growth, conidiation, extracellular protease secretion, and virulence
Cochliobolus heterostrophus	*Cga1*	Appressorium formation and female fertility
Colletotrichum trifolii	*Ctg1*	Vegetative growth, conidial germination, and virulence
Cryphonectria parasitica	*Cpg1*	Colony morphology, female fertility, pigmentation, hydrophobin expression, and virulence
Fusarium oxysporum	*Fga1*	Conidiation, heat resistance, and virulence
Magnaporthe grisea	*MagB*	Vegetative growth, conidiation, appressorium formation, female fertility, and virulence

PAGE). This proteomic approach has led to the identification of several proteins regulated by Gna1 signaling, including Sch1, a short-chain dehydrogenase that is positively regulated. Subsequent genetic dissection of *Sch1* revealed it has a required role in asexual development, a critical facet of disease for this polycyclic pathogen.

MATERIALS AND METHODS

Gene nomenclature. The nomenclature of all *S. nodorum* genes mentioned in this study are denoted by the prefix "SNOG" used in conjunction with the designated gene number. Details of the version 2 annotated sequenced genome can be found at NCBI (http://www.ncbi.nlm.nih.gov/entrez/viewer.fcgi?db=nuccore&id=62183523).

Growth and maintenance of *Stagonospora nodorum*. *S. nodorum* wild-type strain SN15 (Department of Agriculture, Western Australia) and the *gna1-35* strain carrying a disruption in *Gna1* (GenBank accession number EAT82421) were used in this study and were maintained on complex media as described previously (56). For the analysis of the intracellular proteome, 150 mg of fungal mycelia were grown in minimal medium (MM) broth (pH 6.0), which consisted of 30 g liter^{-1} glucose as a carbon source. The fungus was grown to a vegetative phase by incubation at 22°C with shaking at 150 rpm for 3 days. Mycelia were harvested and freeze-dried overnight.

Growth and maintenance of wheat. Growth of *Triticum aestivum* (cv. Amery) and wheat infections were performed as previously described (56).

Protein extraction. For intracellular proteins, freeze-dried mycelia were homogenized with a cooled mortar and pestle with 10 mM Tris (pH 7.6) and 1 mM phenylmethylsulfonyl fluoride. Glass beads (106 μm) of equal volume to the mycelia were used to assist with tissue grinding. The crude homogenate was collected and centrifuged at 20,000 × *g* for 1 h at 4°C. The resulting supernatant was retained and incubated with 20 units of DNase and 20 units of RNase for 1 h at 25°C. Following this, proteins were precipitated with 9 volumes of ice-cold acetone. Precipitated proteins were collected by centrifugation at 4,000 × *g* for 15 min at 4°C and washed with 90% ice-cold acetone. Precipitated proteins were solubilized with multiple surfactant solution, which consisted of 40 mM Tris, 2% (wt/vol) 3-[(3-cholamidoprophyl)-dimethylammonio]-1-propanesulfonate (CHAPS), 2% (wt/vol) sulfobetaine 3-10, 5 M urea, 2 M thiourea, 2 mM tributylphosphine (Bio-Rad), 0.2% (vol/vol) Bio-Lyte 3-10 (Bio-Rad), and 0.002% (wt/vol) bromophenol blue (Bio-Rad). A probe tip Misonix XL2015 sonicator set to an output of 95 W and a 25% s^{-1} pulsar duty cycle was used to assist in protein solubilization. Unless denoted otherwise, all chemicals used were purchased from Sigma-Aldrich.

2D-PAGE. Protein concentration was estimated with a Bio-Rad *RC DC* protein assay kit. For isoelectric focusing, Bio-Rad 7-cm immobilized pH gradient strips were rehydrated with multiple-surfactant solution containing the protein sample (200 μg to 300 μg) in a Bio-Rad Protean isoelectric focusing cell (50 V for 16 h) prior to focusing at 250 V for 15 min and 14,000 V-h (rapid ramping). The proteins in the immobilized pH gradient strip were equilibrated for 20 min with 6 M urea, 0.38 M Tris (pH 8.8), 4% (wt/vol) sodium dodecyl sulfate, 20% (vol/vol) glycerol, and 2% (wt/vol) DTT and a further 20 min in the same buffer that consisted of 2.5% (wt/vol) iodoacetamide substituted for DTT. Equilibrated proteins were separated in a second dimension in manually cast 12% sodium dodecyl sulfate polyacrylamide gels. Gels were visualized via colloidal Coomassie G250 staining (38).

Gel image acquisition and densitometry analysis. Gel images were captured using the ProXpress scanner (Perkin Elmer). Spot detection and gel analyses were performed with the ProGenesis Workstation 2005 software (Linear Dynamics) under default settings. Biological triplicate 2D gels were used to create average gels of the SN15 and *gna1-35* strains for comparisons. Protein spots were considered differentially abundant if the *P* value was <0.05 (unpaired *t* test) and there was a $\geq$2-fold difference in the normalized densitometry value of matching spots between the average gels (see Table S1 in the supplemental material). These spots were excised from gels and the proteins trypsin digested (63).

LC-MS/MS analysis and database searching. Trypsin-digested peptides were analyzed on an Agilent 1100 series capillary LC system coupled to an Applied Biosystems QStar Pulsar *i* liquid chromatography-tandem MS (LC-MS/MS) system equipped with the IonSpray source in positive ion mode (63). Mass spectrum searches were performed with the Mascot search engine, version 2.1.04 (Matrix Science), against the *S. nodorum* predicted protein set at NCBI (http://www.ncbi.nlm.nih.gov/entrez/viewer.fcgi?db=nuccorefid=62183523), utilizing error tolerances of ±1.2 for MS and ±0.6 for MS/MS, "max missed cleavages" set to 1, and the "oxidation (M)" variable modification and peptide charge set at 2+ and 3+. Results were filtered using "standard scoring," "max number of hits" set to 20, "significance threshold" at a *P* value of <0.05, and "ion score cutoff" at 15. Protein matches were considered positive with identifications that contained at least four matching peptides and MOWSE scores of >100. A putative function was assigned to the matched protein by a BlastP homology search of the NCBI nonredundant protein database (minimum expected value cutoff score of 10^{-8}).

RNA isolation and reverse transcription-PCR (RT-PCR). RNA isolation and gene transcript abundance were analyzed as previously described (57). SN15 genomic DNA, prepared with a Retsch MM301 autolyzer and a Qiagen BioSprint 15 workstation, was used as a quantitative standard. Intron-spanning primers (Actin F/R) designed to amplify actin (*Act1* [GenBank accession number EAT90788]) were used to check all cDNA samples and were free of genomic DNA via PCR (data not shown). All primer sequences from this study can be found in Table S2 in the supplemental material.

Gene expression analyses were performed using in vitro-grown fungal tissue and infected wheat leaves. In vitro gene expression analysis of SN15 and the *gna1-35* strain was performed with transcripts extracted under the same growth conditions as those used for the 2D-PAGE analysis. Gene expression was normalized against *Act1* transcript abundance. *Ef1*α is more strongly expressed than *Act1* and was easier to detect on infected wheat leaves where fungal mRNA are limiting, particularly during early infection. Consequently, *Ef1*α was used as the housekeeping gene for the in planta expression studies.

Gene expression between SN15 and the *gna1-35* strain were deemed differentially abundant under the criteria that the *P* value is <0.05 in an unpaired *t* test and there is a $\geq$2-fold difference in the normalized transcript abundances. The expression of putative signaling target genes during SN15 infection on wheat was analyzed with an analysis of variance set for the Tukey-Kramer test in conjunction with a Dunnett's test control. Gene expression was deemed significantly different if the *P* value is <0.05 and there is a $\geq$2-fold difference in the normalized transcript abundances relative to the Dunnett's test control.

Construction of the *Sch1* gene knockout vector. *Sch1* was deleted by gene replacement with a phleomycin resistance selectable marker construct as previously described (54). The 5′ and 3′ untranslated regions (UTRs) of *Sch1* were PCR amplified with the primer pairs 5′FwdXhoI-R567/5′RevHindIII-R567 and 3′FwdPstI-R567/3′RevNotI-R567, respectively. Restriction sites were introduced into the primer sequences to facilitate cloning with the phleomycin resistance selectable marker plasmid vector pBSK-phleo (54). The 5′ *Sch1* UTR amplicon (562 bp) was cloned into XhoI and HindIII sites of pBSK-phleo to produce pBSK-phleo-5′Sch1. The 3′ *Sch1* UTR amplicon (850 bp) was cloned into PstI and NotI sites of pBSK-phleo-5′Sch1 to produce the knockout vector pBSK-Sch1KO. A 3.52-kb gene deletion (knockout [KO]) construct was PCR amplified from pBSK-Sch1KO by using the primer pair R567FwdKO and R567RevKO.

Construction of the *Sch1* promoter-eGFP gene expression construct. The tissue expression pattern of *Sch1* was examined with transcriptional fusion of the putative *Sch1* promoter sequence and an enhanced green fluorescent protein (eGFP) gene. A 1.8-kb 5′ UTR of *Sch1* containing two putative "TATA" Goldberg-Hogness box core promoter sites (30, 52) was PCR amplified with Sch1GFPtransF and Sch1GFPtransR. A partial fragment of pGPD-GFP (49) that consisted of eGFP, a hygromycin resistance cassette, and a *TrpC* terminator was also amplified with GFP-PCRf and GFP-PCRr. Both PCR fragments were fused using the Sch1GFPtransF and GFP-PCRr primers via overlapping PCR (54), with the resulting amplicon used for the subsequent transformation of SN15. PCR was used to test transformants for appropriate ectopic insertions.

Transformation of *S. nodorum*. The protocol for generating protoplasts and genetic transformation of *S. nodorum* SN15 was as previously described (56).

Southern analysis. The PCR amplicon of the primer pair 5′FwdXhoI-R567 and 5′FwdXhoI-R567 was used for random labeling to develop a probe for Southern analysis. This was performed as described elsewhere (56).

Infection assays. Detached leaf and whole plant spray assays were performed as described by Solomon et al. (55).

Histological techniques. Tissues for longitudinal-section histological examination were fixed and degassed overnight in formal acetic alcohol solution in glass vials (48). For embedding in paraffin, tissues were dehydrated in an ascending series of ethanol (70%, 90%, and 100% ethanol; 3 h for each step), then cleared in chloroform prior to infiltration with molten paraffin wax (Paraplast). The embedded tissues were sectioned at 10 μm using Shandon MX35 knives on a Leica RM2235 microtome.

For embedding in Spurr's resin, the fixed tissues were washed in several changes of 0.025 M phosphate buffer and dehydrated in an ascending series of acetone (30%, 50%, 70%, 90%, and 100% acetone; two changes of each solution and 15 min for each change). The tissues were then infiltrated with an ascending series of Spurr's resin (5% to 90%) (62) and then transferred to 100% Spurr's resin for 2 h, and again overnight at room temperature, before being polymerized at 60°C. The embedded tissues were sectioned at 1 μm on a Reichert Jung 2050 microtome.

The double-stranded-DNA-specific stain 4′,6-diamidino-2-phenylindole dilactate (DAPI) was used to stain paraffin tissue sections according to the manufacturer (Invitrogen). A mixture of 1% methylene blue and 1% azur II in 1% sodium tetraborate solution was used as a general stain as described elsewhere (47).

For transmission electron microscope (TEM) analysis, tissues embedded in Spurr's resin were sectioned at 80 nm using a diamond knife on a Reichart Ultracut E ultramicrotome. The sections were mounted onto 200-mesh copper grids (ProSciTech), stained for 20 min in a saturated aqueous solution of uranyl acetate, washed twice in distilled water, then stained in lead citrate for 4 min and washed again with several changes of distilled water (65). The stained sections were examined at 80 kV on a Philips CM100 biotransmission electron microscope.

For eGFP analysis, mycelia containing pycnidia of the *Sch1*-eGFP transformant grown on CzV8CS agar were excised and longitudinally hand-sliced with a double-edge stainless-steel razor blade. Sections were viewed under differential interference contrast (DIC) and blue-light excitation (460 to 490 nm) for eGFP fluorescence. Composite images were constructed with the DPManager software (Olympus).

GenBank accession numbers. Broad-annotated genes analyzed in this study are available in the GenBank/EMBL databases under the accession numbers EAT82552 (*Sch1*/SNOG_10217), EAT85007 (SNOG_07541), EAT85070 (SNOG_07604), EAT79369 (SNOG_13042), EAT81580 (SNOG_11081), EAT81149 (SNOG_11441), and EAT84551 (SNOG_08275).

RESULTS

Comparative proteomic analysis and identification of genes that correspond to the differentially abundant proteins. The intracellular proteomes of SN15 and the *gna1-35* strain were separated by 2D-PAGE (Fig. 1A and B). A total of 475 unique protein spots were identified in the SN15 and *gna1-35* strain samples. Of these, six spots were identified as being >2-fold different in abundance ($P < 0.05$). Five spots (C1 to C5) were significantly less abundant, and one spot (C6) showed an increase in abundance in the *gna1-35* strain. LC-MS/MS analysis was used to obtain spectra of peptides derived from these protein spots, and the resulting data were matched against those of the *S. nodorum* predicted protein set to find the matching genes (Table 2). Seven genes were identified from the six differentially abundant protein spots. Proteins identified from spots C1 to C5 matched to genes that code for a putative concanamycin-induced protein C (*CipC*; SNOG_11081), a glutathione *S*-transferase (SNOG_07604), short-chain dehydrogenases (SNOG_10217 and SNOG_13042), and a proteasome subunit (SNOG_07541). Two proteins (C6-1 and C6-2) were identified from spot C6 and matched to genes that code for 3-dehydroquinate dehydratase (SNOG_11441) and a protein of unknown function (SNOG_08275).

Transcriptional analysis of putative heterotrimeric G protein signaling target genes. The expression of genes encoding putative heterotrimeric G protein signaling target proteins was examined with RT-PCR. This was performed to determine whether protein abundance was regulated at the transcriptional or posttranscriptional level. The normalized expression of each gene was compared with protein abundance data to identify relative correlations of protein and transcript abundances. Of the seven genes examined, four showed a positive correlation between protein and transcript abundances, implying that these genes are regulated at the transcriptional level (Fig. 2). Three of these genes (SNOG_13042, SNOG_10217, and SNOG_11081) showed transcriptional downregulation, whereas one (SNOG_11441) was upregulated in the *gna1-35* strain. The other three genes (SNOG_07541, SNOG_07604, and SNOG_08275) showed no correlation between protein and transcript abundances.

Quantitative RT-PCR was also used to determine the expression profiles of these genes in *S. nodorum* during infection of wheat. Sampling time points were 1, 3, 5, and 8 days postinfection, which coincided with host penetration, proliferation, onset, and late pycnidiation, respectively (61). Six of the genes identified from the proteomic analysis showed significantly differential expression during infection of detached wheat leaves by *S. nodorum* (Fig. 2). Five of these (SNOG_07541, SNOG_07604, SNOG_10217, SNOG_11441, and SNOG_13042) showed increased expression during late infection coinciding with asexual sporulation. One gene (SNOG_11081) was significantly more expressed during germination and penetration of the host at 1 day postinfection. No expression was detected for SNOG_08275 during in planta growth.

SNOG_10217 encodes a putative short-chain dehydrogenase. The focus of this study was to identify and functionally characterize targets of Gna1-dependent regulation. SNOG_10217 was chosen for further analysis based on its strong downregulation in the *gna1* strains. The open reading frame of SNOG_10217 consists of two introns and encodes a polypeptide of 299 amino acids with a predicted molecular mass and pI of 31.8 kDa and 5.5, respectively. These predicted figures closely match the experimental molecular mass and pI as described above. SNOG_10217 contained a Pfam domain of the short-chain dehydrogenase family, thus the gene was subsequently named *Sch1*. Sch1 also possesses signature short-chain dehydrogenase motifs with inferred function in coenzyme binding (T-G-V-S-G-G-I-G [residues 44 to 51]) and structural stabilization sequences (N-N-A-G [residues 125 to 128]) (41). BlastP (1) analysis of Sch1 revealed significant matches to

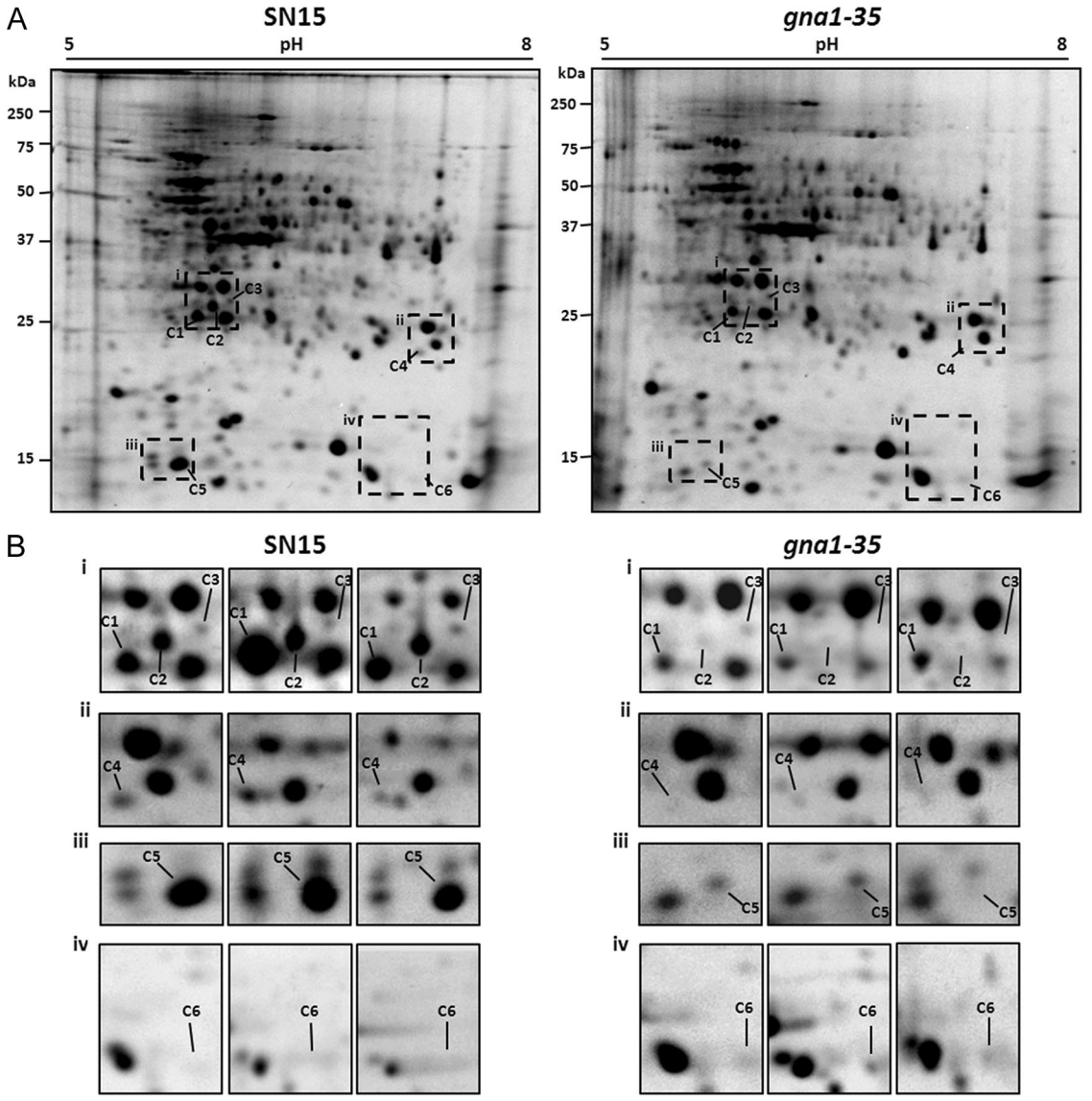

FIG. 1. (A) Representative 2D-PAGE gels of the SN15 and *gna1-35* strains showing differentially abundant proteins in the intracellular proteomes. (B) Subpanels of the regions marked in panel A for each of the biological triplicate samples. Gels representing each of the biological triplicates are available in Fig. S4 in the supplemental material.

hypothetical fungal short-chain dehydrogenases (40% to 50% amino acid identities).

***Sch1* is highly expressed in pycnidia.** Examination of gene expression by quantitative PCR showed that *Sch1* transcript abundance was maximal during the latter stages of infection, implying a role for Sch1 in asexual sporulation. To gain a more detailed understanding of expression during asexual development, a transcriptional fusion consisting of the *Sch1* 5′ putative promoter region fused to the eGFP gene was constructed and transformed into SN15. Subsequent transformants were screened with those demonstrating phenotype and pathogenicity comparable to those of the *S. nodorum* wild type, chosen for further analysis (data not shown). eGFP expression was examined in vitro by excising hyphae and pycnidia from the transformed strain growing on complex CzV8CS agar (Fig. 3). Images collected by DIC microscopy showed asexual sporulation occurring at various stages of development on the agar. Examination of these samples for eGFP expression highlighted that fluorescence was localized strictly to within mature pycnidia or differentiating asexual structures, known as mycelial knots. Fluorescence was not observed in vegetative mycelia. Higher-magnification data revealed that eGFP expression was observed in the pycnidial cavity that consisted of the subparietal tissue layer and asexual pycnidiospores but not the melanized pycnidial wall. These results confirm the strong expression of *Sch1* during asexual development and demonstrate the specificity of the expression in the sporulation structures.

Targeted gene deletion of *Sch1*. The eGFP expression analysis highlighted a potential role for Sch1 in asexual development. Mutants of *S. nodorum* lacking *Sch1* were created by homologous recombination with an *Sch1* gene deletion construct conferring phleomycin resistance (Fig. 4A). Initial PCR screening enabled

TABLE 2. Identification of differentially abundant proteins with LC-MS/MS and Mascot

Spot	Difference[a]	SNOG	Putative identity	Observed pI; predicted pI	Observed pI; predicted M_r (kDa)	MOWSE score; peptide no. (% coverage)	Signal peptide[b]	Transcript correlation[c]
C1	−2.7	13042	Short-chain dehydrogenase	5.81; 5.41	27.1; 28.9	748; 20 (52)	N	Y
C2	−17.5	10217	Short-chain dehydrogenase	5.94; 5.46	28.5; 31.8	696; 16 (55)	N	Y
C3	−7.2	07541	Proteasome component	6.06; 6.20	29.2; 27.9	256; 7 (37)	N	N
C4	−3.5	07604	Glutathione transferase	7.43; 6.53	23.3; 24.4	128; 4 (24)	N	N
C5	−19.2	11081	Concanamycin-induced protein C (CipC)	5.70; 5.21	<15.0; 15.1	386; 10 (60)	N	Y
C6-1	+4.7	11441	3-dehydroquinate dehydratase	7.43; 6.49	<15.0; 16.5	223; 6 (37)	N	Y
C6-2	+4.7	08275	Unknown	7.43; 6.13	<15.0; 14.7	205; 6 (44)	N	N

[a] Differences of matching protein spots are calculated from the normalized spot value of SN15 relative to that of the *gna1-35* strain.
[b] N, no.
[c] Refer to Fig. 2. Y, yes; N, no.

the recovery of two independently derived gene deletion mutants designated as *S. nodorum sch1-11* and *sch1-42* mutants and an ectopic strain designated as the *Sch1-30* mutant. Southern analysis confirmed the presence of *Sch1* in the *Sch1-30* mutant and successful gene deletion in the *sch1-11* and *sch1-42* mutants (Fig. 4B). 2D-PAGE of the transformants confirmed that the protein spot corresponding to Sch1 was present in the SN15 and *Sch1-30* strains but not in the *sch1* mutants (Fig. 4C). This indicates a correct protein-to-gene assignment via MS identification and unequivocal evidence of gene deletion.

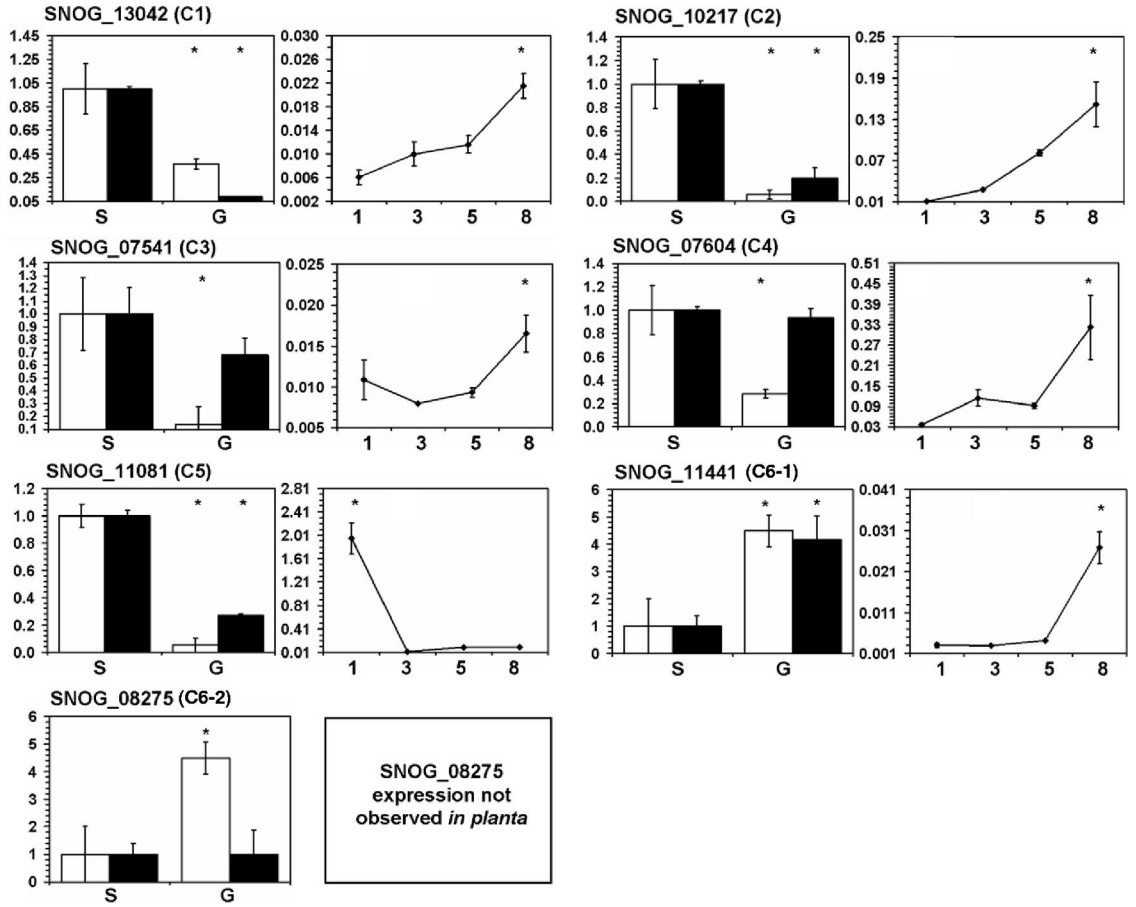

FIG. 2. Protein/transcript abundance graphs for each of the targets identified via 2D-PAGE. The transcript profiling of each gene is comprised of two panels. The panels on the left are a comparison of relative protein (white bars) and transcript (black bars) levels for each of the targets in vitro. Asterisks located on top of bar graphs signify significant differences in protein and transcript abundances. "S" and "G" on the *x* axis denote the SN15 and *gna1-35* strains, respectively. The panels on the right (line graphs) depict gene expression in planta for each target gene. Numbers on the *x* axis are the number of days postinfection, and asterisks denote differential gene expression relative to the Dunnett's test control group. The *y* axis represents relative gene expression levels normalized to *Act1* (in vitro) or *Ef1*α (in planta). Standard error bars are shown.

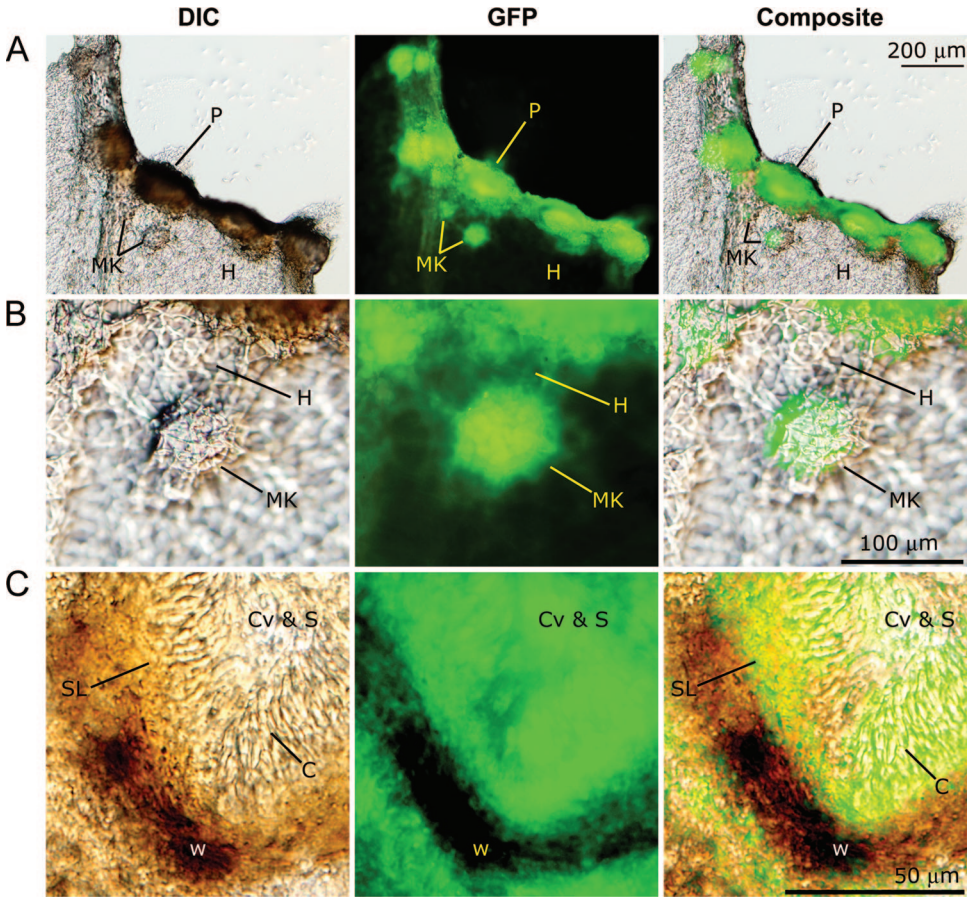

FIG. 3. Expression of the *Sch1* promoter-eGFP fusion construct in SN15. Longitudinal section images taken with DIC microscopy showing hyphae and mature and immature pycnidia (mycelial knots). Panels A, B, and C represent increasing magnifications. C, conidiogenous cell; Cv, pycnidial cavity; H, hyphae; MK, mycelial knot; P, pycnidium; S, spore; SL, subparietal layer; W, pycnidial wall.

***Sch1* deletion affects vegetative growth.** Vegetative growth of the *sch1* strains was compared with those of the SN15 and *Sch1-30* strains on solid agar media. All strains examined demonstrated a similar radial growth rate on complex CzV8CS agar as that of the *sch1* mutants, producing a green pigment in older mycelia (Fig. 5A). When grown on defined MM agar, the *sch1* mutants showed a significant reduction in radial growth compared to both the SN15 and *Sch1-30* strains. The inclusion of components from the complex media in the MM agar failed to complement the growth defect, implying that the phenotype is more than a simple auxotrophic response. The vegetative phenotype of the *sch1* mutants was also investigated when grown as submerged cultures in shaking flasks consisting of MM broth. At 24 h postinoculation, the mycelia of both SN15 and the ectopic mutant were dispersed throughout the media as is typically observed. The mycelia of the *sch1* strains were not dispersed but appeared to aggregate into a single mass (data not shown).

Based on the phenotypic variation apparent from these simple in vitro growth assays, we attempted to complement the mutation by reintroducing the *Sch1* gene into the *sch1* strain background. Attempts to generate the required number of *sch1* protoplasts proved difficult, most likely due to the clumping phenotype observed in the shaking flasks. Assays in multiple flasks were attempted to generate sufficient protoplasts, but this, too, was unsuccessful. Consequently, genetic complementation of the *sch1* strains was not possible.

***Sch1* is dispensable for proliferation on wheat.** The *sch1* mutants were examined for their ability to cause lesions on wheat. A detached-leaf assay was used to measure the progress of lesion development from a single point inoculation over a 14-day period. Lesion sizes caused by all fungal strains on detached wheat leaves were not significantly differently (data not shown). A whole plant spray assay was also used to simulate a field infection by spraying spore suspensions onto 2-week-old wheat plants. The disease scores for all strains were comparable indicating that *Sch1* is dispensable for lesion development on wheat (data not shown).

***Sch1* deletion affects asexual sporulation in vitro and in planta.** The eGFP-fusion experiments revealed the localized nature of *Sch1* expression during asexual development. Also apparent from the subculturing and harvesting of the *sch1* strains was the very low numbers of spores recovered. To analyze the sporulation phenotype further, pycnidiospores of all strains were harvested and compared via light microscopy analysis (Fig. 5B). Spore suspensions derived from SN15 and the *Sch1-30* strain were predominantly composed of pycnidiospores. The spore suspensions harvested from the *sch1* strains

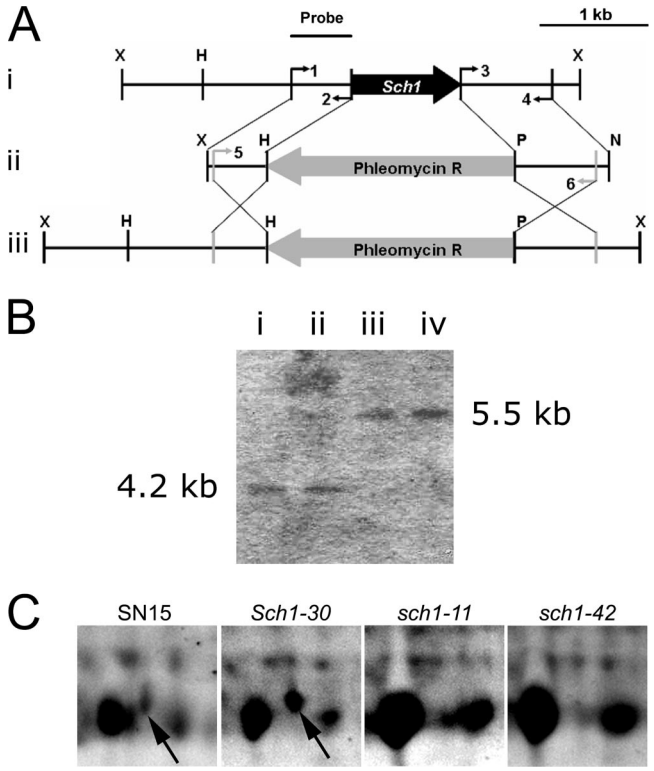

FIG. 4. Construction of the *sch1* mutants. (A) (i) The *Sch1* knockout vector was constructed by ligating PCR-amplified 5′ and 3′ UTRs of *Sch1* to the XhoI/HindIII and PstI/NotI restriction sites of pBSK-phleo, respectively. (ii) The knockout vector was PCR amplified and transformed into SN15 to facilitate homologous gene replacement, as shown in panel iii. Restriction sites are as follows: X, XhoI; H, HindIII; P, PstI; and N, NotI. Primers are as follows: 1, 5′FwdXhoI-R567; 2, 5′RevHindIII-R567; 3, 3′FwdPstI-R567; 4, 3′RevNotI-R567; 5, R567 FwdKO; and 6, R567RevKO. Primer sequences are listed in Table S2 of the supplemental material. The probe used for Southern analysis is indicated. (B) Southern analysis of the *S. nodorum* SN15 (i), *Sch1-30* (ii), *sch1-11* (iii), and *sch1-42* (iv) strains. Bands corresponding to 4.2 and 5.5 kb were predicted for strains carrying an intact or deleted gene, respectively. Genomic DNA was digested with XhoI prior to blotting. (C) Detection of Sch1 (arrows) via 2D-PAGE.

contained far fewer spores and much of what was assumed to be mycelial debris. Quantitative analysis of the spores harvested showed an approximately 50-fold decrease in the number produced by the *sch1* strains (Fig. 6C). Significantly fewer pycnidiospores were also produced by the *sch1* strains in planta, implying that the phenotype is not restricted to a specific growth environment (Fig. 6D). The *sch1* deletion also resulted in reduced average spore length (Fig. 6E), although the germination rate of the mutants was unaffected (data not shown).

***Sch1* is required for pycnidial development in vitro and in planta.** Abnormalities in asexual sporulation of the *sch1* mutants prompted further studies of the mutant pycnidia. The pycnidia of SN15 and the *Sch1-30* strain exuded a pink cirrhi when grown on CzV8CS agar, while the cirrhi secreted by the *sch1* pycnidia appeared much paler, almost white, and less abundant (Fig. 6A). On wheat leaves, the mutant phenotype was further exaggerated with the *sch1* strains not exuding visible cirrhi from the pycnidia (Fig. 6B). The diameter of *sch1* pycnidia was also significantly smaller than those of the wild-type or ectopic strains both in vitro and in planta, suggesting a structural role for Sch1 (Fig. 6C and D).

The ontogeny of SN15 and *sch1-42* pycnidia in vitro was compared via tissue longitudinal sectioning and visualization with DIC, bright field, and TEM (Fig. 7A). Immediately apparent was the smaller size of the *sch1* pycnidium, confirming the measurements reported above. Within the pycnidial cavity, far fewer pycnidiospores were present for the mutant, which is consistent with the much lower density of spores demonstrated in the exuding cirrhus. The cell walls of the two strains were also structurally different, with the cells within the SN15 wall appearing to be more uniform than the corresponding cells in the *sch1-42* strain.

The pycnidia of the *sch1-42* strain showed similar developmental defects during growth on wheat leaves (Fig. 7B). The contents of the pycnidial cavity again significantly differed with that of the cavity of the wild type, comprising of tightly packed uniform spores. Surrounding the cavity is the subparietal layer that lines the inner wall of the pycnidium. The subparietal layer was evident in SN15 as a dense ring enveloping the cavity but was poorly defined for the *sch1* strain. It was further observed that the conidiogenous cells in the *sch1-42* strain were unable to differentiate into distinct pycnidiospores. As witnessed for the in vitro samples, the pycnidial wall cells of SN15 and the *sch1-42* strain were morphologically different, as indicated by the staining pattern.

TEM analysis was used to interpret the structural alteration of *sch1* pycnidia in greater detail (Fig. 7B, panels iii and vi). It was observed that a substantial portion of most SN15 pycnidial wall cells was occupied by a vacuole. Electron-dense materials, presumed to be cytoplasmic constituents, were often located adjacent to the intracellular side of the cell wall. In contrast, corresponding cells in the *sch1-42* strain contained multiple small vacuoles and a high proportion of cytoplasmic constituents.

It was observed that the pycnidia of the *sch1-42* strain resembled previously described immature pycnidia of *S. nodorum* (10). Hence, it was possible that Sch1 may be involved in the differentiation of the pycnidial primordium to maturity. To test this hypothesis, SN15 (mature and developing) and *sch1-42* pycnidia were examined for nuclei distribution using DAPI staining (Fig. 8). The mature SN15 subparietal layer was distinguishable from the cell wall, as the latter tissue revealed comparatively less nuclei. Nuclei were also observed in spores located in the pycnidial cavity amid the background fluorescence. The pycnidial cell wall and subparietal layer of the *sch1-42* strain were indistinguishable, as the DAPI staining indicated that most cells surrounding the pycnidial cavity were nucleated. DAPI staining of an immature pycnidium of SN15 showed a similar nuclei distribution pattern as that of the *sch1-42* strain (Fig. 8). Collectively, these data suggest that the pycnidial wall of the *sch1-42* strain may be attenuated in pycnidial maturation.

Sch1 regulation is independent of Ca^{2+}/calmodulin signaling. Sch1 abundance was examined in previously characterized signaling mutant strains lacking the MAP kinase Mak2 and the Ca^{2+}/calmodulin protein kinase CpkA (54, 59). The level of Sch1 protein in the *cpkA* strain was not significantly different from that in SN15, suggesting that the regulation of Sch1 is

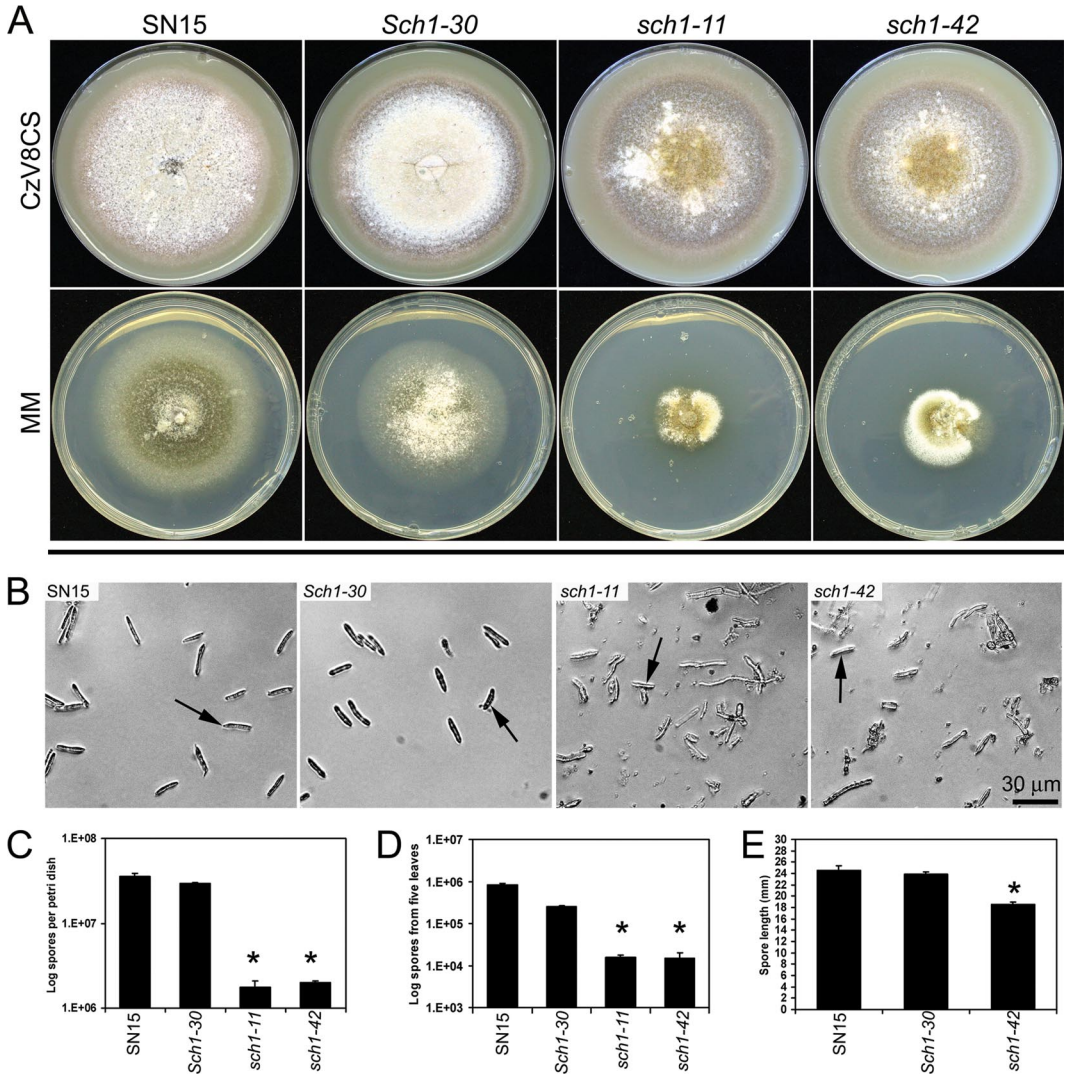

FIG. 5. Vegetative morphology of the *sch1* mutants. (A) Colony morphology after 2 weeks of growth on CzV8CS and MM agars. (B) Light microscope images of pycnidiospores (arrows) harvested from the *S. nodorum* SN15, *Sch1-30*, *sch1-11*, and *sch1-42* strains. Notice the mycelial debris associated with the spores of the *sch1* mutants. (C) Spores per plate from strains grown on CzV8CS agar for 2 weeks. Mean values were calculated from three spore counts of biological pooled plate replicates of the SN15 ($n = 3$), *Sch1-30* ($n = 3$), *sch1-11* ($n = 11$), and *sch1-42* ($n = 12$) strains. (D) In planta sporulation assay results. Mean values were calculated from three spore counts of pooled spores derived from biological infected replicates of the SN15 ($n = 10$), *Sch1-30* ($n = 10$), *sch1-11* ($n = 5$), and *sch1-42* ($n = 5$) strains. (E) A comparison of the average spore length of the SN15, *Sch1-30*, and *sch1-42* strains ($n = 34$). Note that asterisks denote a significant difference to SN15 ($P < 0.05$).

independent of the Ca^{2+}-/calmodulin-dependent signaling (Fig. 9). The amount of Sch1 protein was significantly less in the *mak2* strain than in SN15 but was comparable to the level observed in the *sch1-42* strain, suggesting that the Mak2 MAP kinase signaling pathway has a role in the regulation of Sch1.

DISCUSSION

We have previously shown that inactivation of Gna1 has resulted in extensive changes in the phenotype and pathogenicity *S. nodorum*. Hence, the aim of this study was to identify and functionally characterize proteins in the pathogen *S. nodorum* that are regulated by signaling events associated with the $G\alpha_i$ subunit Gna1.

2D-PAGE was used to directly compare the intracellular proteomes of the *gna1* and *S. nodorum* wild-type strains. The analysis of the 2D-PAGE data set led to the identification of seven intracellular proteins that were regulated at a significant level by Gna1 in biological independent samples analyzed in triplicate. The subsequent data were subjected to rigorous statistical analysis with only proteins with significant differences reported. A less stringent approach would have resulted in the identification of many more "regulated" proteins, but their biological significance would have been questionable.

The seven genes identified encode putative proteins of diverse function. SNOG_11081 encodes a putative concanamycin-induced protein C. CipC was first identified as an accumulated protein in *Aspergillus nidulans* exposed to the antibiotic concanamycin A (36). Orthologues of *CipC* were also identified in other fungi; however, their function is unknown (2, 29,

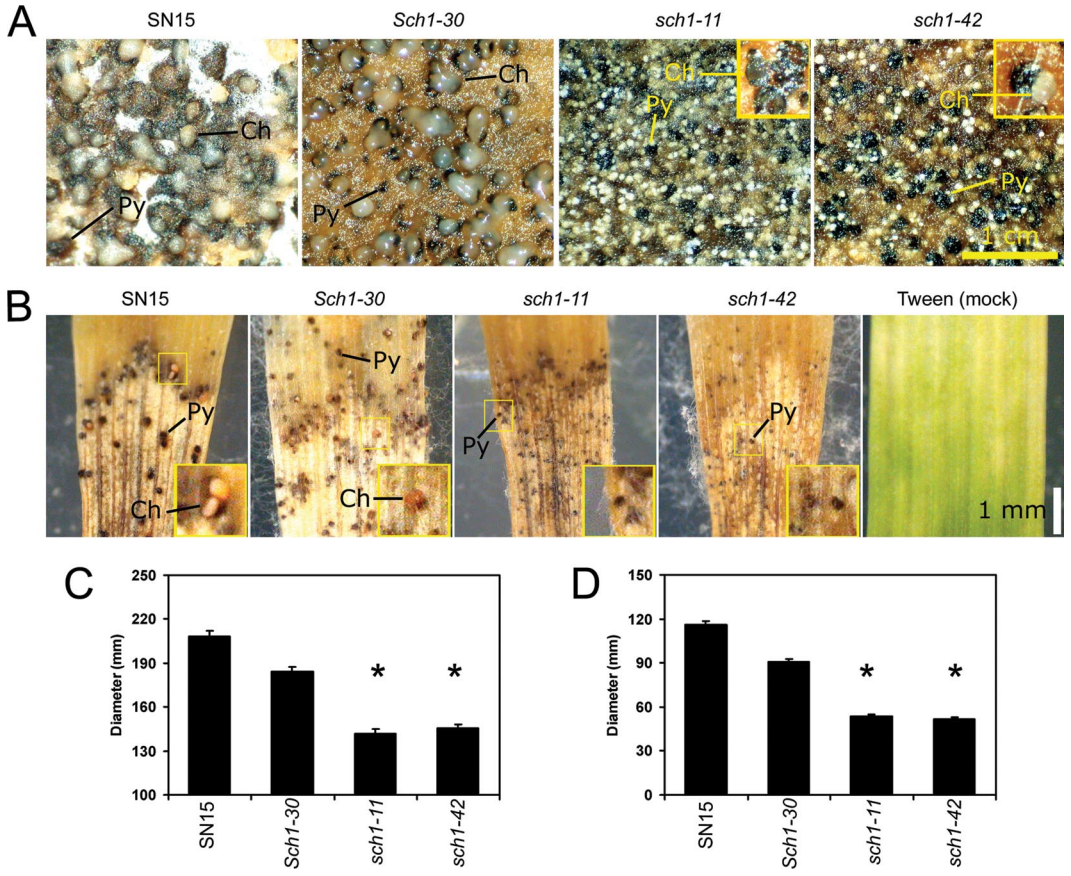

FIG. 6. *Sch1* deletion affects pycnidial function and size. Digital images of pycnidia produced on CzV8CS agar (A) and wheat leaves (B). Pycnidia of the *sch1* mutants rarely exude spores. Ch, cirrhus; Py, pycnidium. The average diameter of pycnidia derived from growth on CzV8CS agar (the SN15 [$n = 191$], *Sch1-30* [$n = 146$], *sch1-11* [$n = 144$], and *sch1-42* [$n = 286$] strains) (C) and wheat leaves (the SN15 [$n = 69$], *Sch1-30* [$n = 69$], *sch1-11* [$n = 151$], and *sch1-42* [$n = 184$] strains) (D). Note that asterisks denote a significant difference to SN15 ($P < 0.05$).

37, 43, 64). The gene expression profile of *CipC* in planta showed maximal transcript abundance 1 day postinfection, which suggests that this gene may play a role during early infection. Gene disruption of SNOG_11081 had no effect on the pathogenicity or phenotype of *S. nodorum* (data not shown). SNOG_07694 and SNOG_13042 encode a putative glutathione *S*-transferase and a short-chain dehydrogenase, respectively. These, too, were subsequently characterized by gene disruptions. The resulting mutants appeared to be identical to the wild-type strain, implying that these genes, while regulated by *Gna1*, did not significantly contribute to the phenotype of the *gna1* strains (data not shown).

The disruption of a fourth gene, SNOG_10217, generated strains of *S. nodorum* unable to differentiate mature pycnidia. Sequence analysis of SNOG_10217 identified it as also belonging to the family of short-chain dehydrogenase, and the gene was subsequently named *Sch1*. The pycnidia developed by *sch1* strains were smaller and contained a significantly lower number of pycnidiospores which appeared abnormal in shape. Histological analysis of these mutant pycnidia highlighted significant structural differences compared to the wild type, including the spore density and the shape within the pycnidial cavity and also structural deformity of the subparietal layer and pycnidial wall.

It was observed that the protein sequences of Sch1 and SNOG_13042 shared approximately 30% similarity. On this basis, we investigated whether SNOG_13042 was partially compensating for the loss of Sch1 in the *sch1* strains via the creation of a double mutant lacking both *Sch1* and *Sch2*. The resulting mutants were identical to the *sch1* strains, strongly suggesting that Sch2 is not compensating for the loss of Sch1 (see Fig. S3 in the supplemental material).

There have been several recent reports examining the molecular and biochemical requirements of asexual sporulation in *S. nodorum.* The cAMP-dependent (*Gna1*), MAP kinase (*Mak2*), and calcium (*CpkA*) signaling pathways all have a demonstrated role in sporulation (54, 56, 59). Analyses in this study have shown that Sch1 is regulated by *Gna1* and *Mak2* but not *CpkA*. Shared regulation by the cAMP-dependent and MAP kinase signaling pathways was not unexpected, as cross talk between these pathways has been well documented (23, 40).

The presence of the sugar alcohol mannitol has also been identified as a requirement for *S. nodorum* to undergo asexual sporulation (55, 58, 60). The levels of mannitol appear unchanged when comparing the *sch1* strains with SN15, excluding it as having a role in the *sch1* defect (data not shown). Hence,

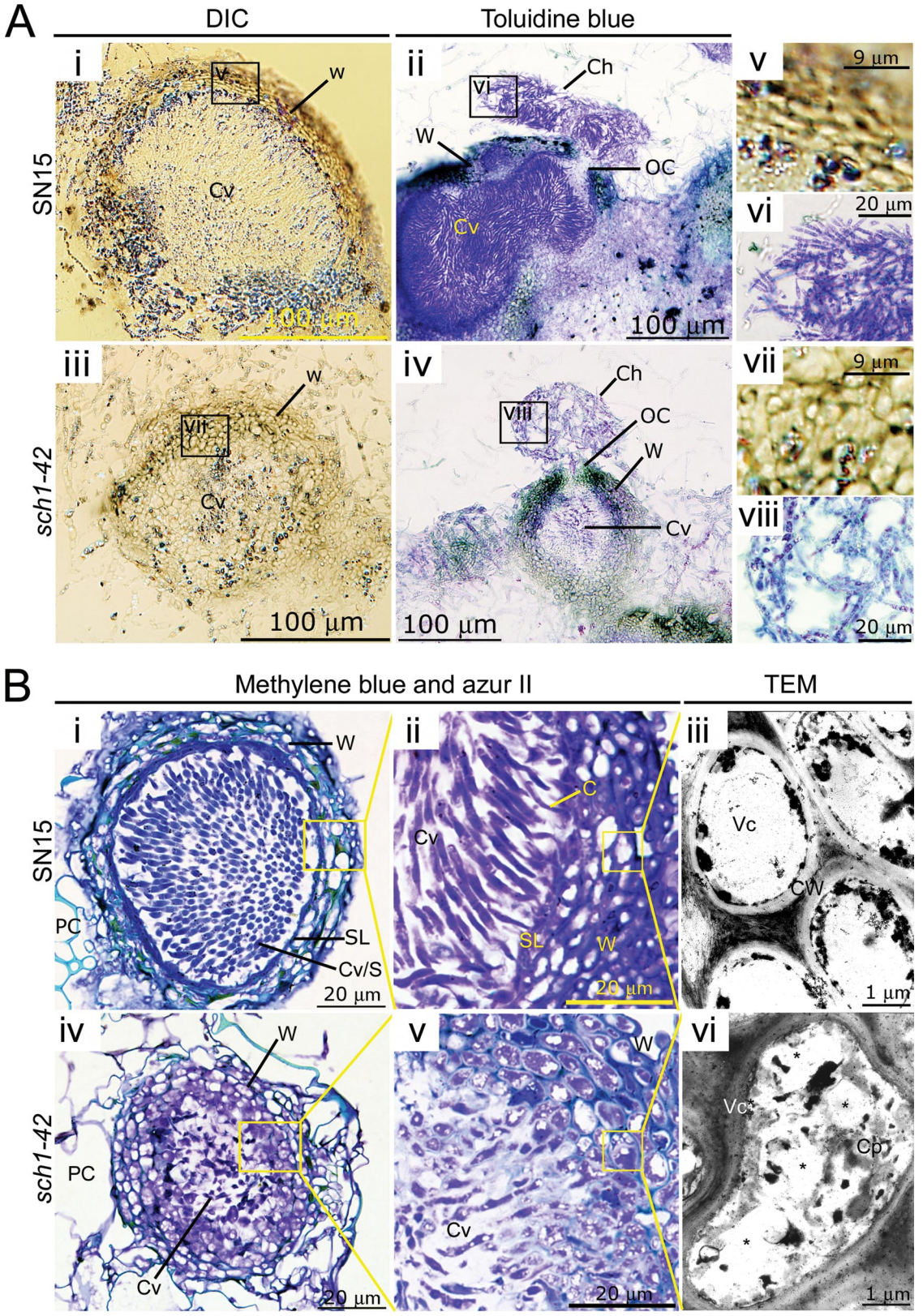

FIG. 7. Analysis of SN15 and *sch1-42* pycnidia via longitudinal sectioning. (A) The morphology SN15 and *sch1-42* melanized pycnidial wall (panels i and iii) and cirrhi (panels ii and iv) are demonstrated via paraffin embedding and sectioning. Magnified images of the unstained pycnidial wall cellular arrangements (panels v and vii) and cirrhi (panels vi and viii) are shown. (B) Spurr's resin embedding sectioning of SN15 (panels i, ii, and iii) and *sch1-42* (panels iv, v, and vi) pycnidia showing greater details of cells of the pycnidial wall and the subparietal layer. Panels i and iv show pycnidia of the SN15 and *sch1-42* strains. Panels ii and v are images taken from increased magnifications of the pycnidial wall and cavity interface of SN15 and *sch1-42* pycnidia. Cells of the pycnidial wall were examined via a TEM (panels iii and vi). C, conidiogenous cell; Ch, cirrhus; Cp, cytoplasm; Cv, pycnidial cavity; N, nucleus; PC, plant cell; OC, ostiolar cone; S, spore; SL, subparietal layer; Vc, vacuole; W, pycnidial wall.

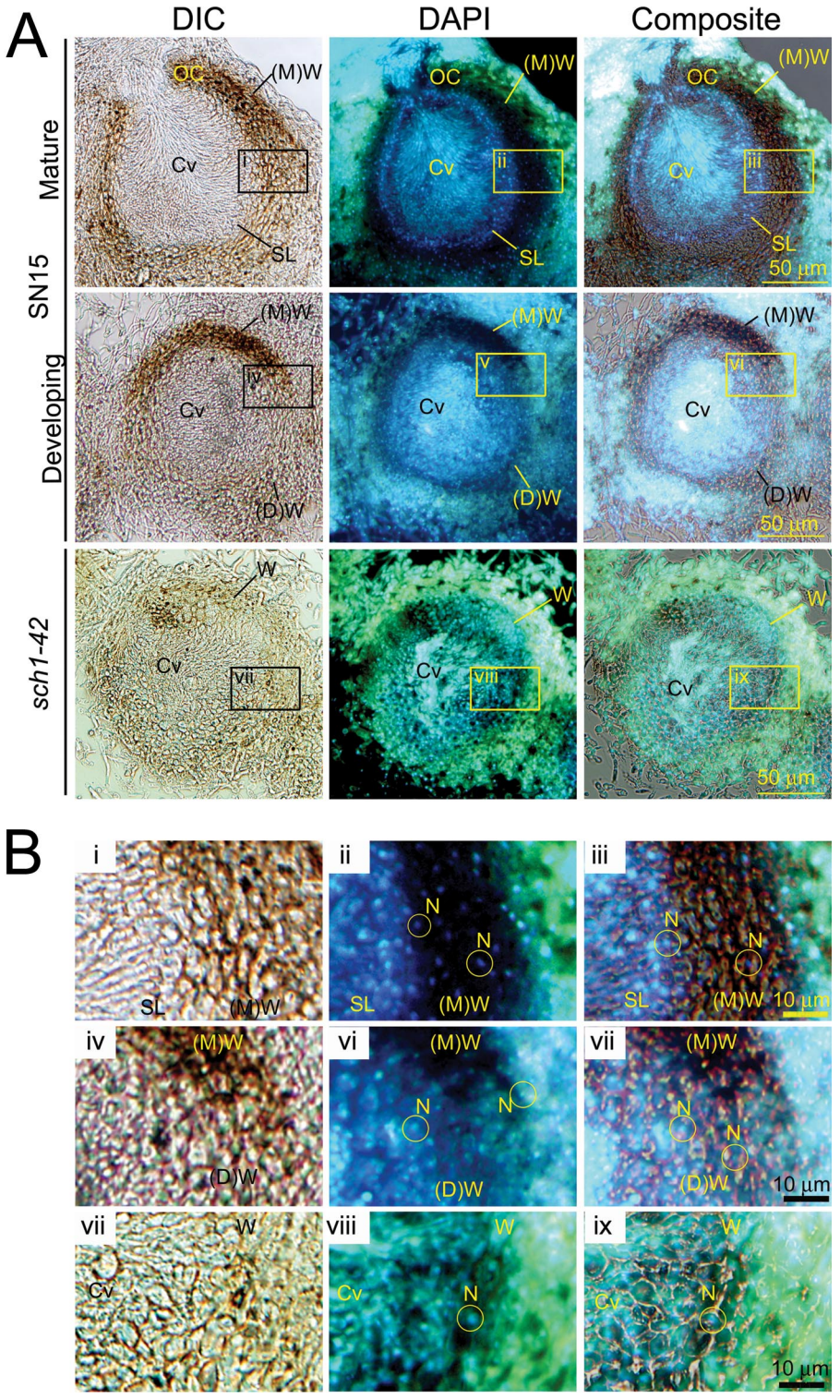

FIG. 8. The nuclear content of SN15 and *sch1-42* pycnidia was examined from longitudinal tissue sections stained with DAPI. (A) A comparison of nuclei distribution in pycnidia of SN15 at different stages of development and in that of the *sch1-42* strain. Boxes are expanded in panel B, showing a greater magnification of the DAPI-stained cell wall and subparietal-layer regions of SN15 and *sch1-42* pycnidia. Cv, pycnidial cavity; N, nucleus; OC, ostiolar cone; SL, subparietal layer; Vc, vacuole; W, pycnidial wall; (D), developing; (M), mature.

Sch1 appears to be a novel factor in *S. nodorum* that is required for appropriate sporulation.

Douaiher et al. have previously reported the ontogeny of *S. nodorum* pycnidia in vitro (10). This detailed examination elegantly described the differentiation of a pycnidium from the initial formation of the mycelial knot through to a fully mature structure. A comparative analysis of these structures described by Douaiher et al. with those produced by the *sch1* strains

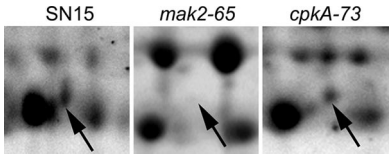

FIG. 9. Representative regions of 2D gels from the *S. nodorum* SN15, *mak2-65*, and *cpkA-73* strains. The arrows indicate the presence/absence of Sch1.

indicates that differentiation of the *sch1* pycnidia is interrupted through the development of the pycnidial primordium. This stage has been defined as the formation and the extension of the pycnidial cavity and conidiogenesis. A pycnidial cavity has clearly formed for the *sch1* structures, but the conidiogenesis cells are difficult to distinguish. Furthermore, using DAPI staining, we have shown that the walls of *sch1-42* pycnidia contain a similar nuclei distribution to that of an immature pycnidium of SN15. Hence, the evidence reported here indicates that the *Sch1* gene/product has a discrete role in this stage of pycnidial development.

Many important phytopathogenic fungi, such as *C. parasitica*, *Cochliobolus heterostrophus*, and *Mycosphaerella graminicola*, are capable of asexual sporulation through pycnidia. Recent studies have identified various signaling pathways as having a role in pycnidial development in these fungi (6, 35). Similar studies in *S. nodorum* also identified that the calcium-/calmodulin-dependent protein kinase CpkA was required for proper pycnidial differentiation (54). However, the genes and proteins regulated by these signaling pathways that are required for the development of wild-type pycnidia are yet to be identified. To our knowledge, *Sch1* is the first signal transduction target identified to play a required role in the development of pycnidia.

Three additional genes were identified during the course of this study, as regulated by G protein signaling, but have yet to be functionally characterized. SNOG_07541 encodes an alpha type 2 proteasome subunit which comprises part of the 20S proteasome, the central enzyme of nonlysosomal protein degradation in both the cytosol and nucleus (34). SNOG_08275 encodes a protein of unknown function that is not expressed during infection, while SNOG_11441 encodes a putative dehydroquinate dehydratase. The 3-dehydroquinate dehydratase protein is associated with quinate metabolism (15). In *Neurospora crassa*, Qa-2p is required for the conversion of 3-dehydroquinate to 3-dehydroshikimate. Both compounds are intermediates of aromatic amino acid biosynthesis and quinate catabolism pathways (15, 20). It is possible that the increased abundance of the Qa-2p orthologue in *S. nodorum* may have led to a perturbation of the aromatic amino acid pathway. This in turn may have affected dihydroxyphenylalanine melanin biosynthesis in the *gna1* strains and resulted in the albino vegetative phenotype previously reported. However, this hypothesis requires further investigation.

A thorough gene expression analysis, both in vitro and in planta, was undertaken on the genes encoding the seven proteins. Quantitative transcript measurements revealed a correlation between protein and transcript abundances in four of the seven genes. Three of the genes were downregulated in the *gna1* background, while one was upregulated. The protein and transcript abundances in the three remaining genes did not correlate in vitro. Similar observations were previously made in studies of other biological systems using both proteomics and transcriptomics to analyze gene expression (13, 18). This may be attributed to posttranscriptional regulation or differing half-lives of transcripts and proteins (26, 33). Nevertheless, some of these genes showed a differential expression pattern during infection, suggestive of transcriptional regulation by unknown factors.

This study has demonstrated that 2D-PAGE is an effective method for analyzing the proteomes for downstream targets of signaling pathways that are differentially accumulated between *S. nodorum* SN15 and *gna1* strains. The genes encoding several of these proteins were functionally characterized by gene disruption. Through this approach, the short-chain dehydrogenase Sch1, which is subjected to positive regulation by Gna1, was found to be required for the differentiation of pycnidia. *S. nodorum* is a polycyclic pathogen, and, as such, asexual sporulation is an attractive target for investigating mechanisms of disease control. It is relevant to note that, although deformed, the *sch1* strains were able to form pycnidia. In contrast, the *Gna1* mutants were unable to differentiate pycnidia, suggesting that additional unidentified signaling targets are required to initiate pycnidial formation from precursor hyphal cells. It should also be considered that proteome changes observed in this study may have been the result of perturbation in other parts of the heterotrimeric G protein pathway, rather than Gna1 alone. Therefore, the proteins identified could have been directly or indirectly regulated by Gna1.

We anticipate that this study will stimulate research to further understand the biology of pycnidial development in other fungal pathogens and its requirement for the establishment of diseases.

ACKNOWLEDGMENTS

We thank Kasia Rybak and Eva Antoni for technical assistance and Barbara J. Howlett at The University of Melbourne for providing the pGPD-GFP construct. This research was supported by the Grains Research and Development Corporation.

K.-C.T. was supported by an Australian Postgraduate Award. J.L.H. and A.H.M. were supported by an ARC Australian Postdoctoral Fellowship and an ARC Australian Professorial Fellowship, respectively.

REFERENCES

1. **Altschul, S. F., T. L. Madden, A. A. Schaffer, J. Zhang, Z. Zhang, W. Miller, and D. J. Lipman.** 1997. Gapped BLAST and PSI-BLAST: a new generation of protein database search programs. Nucleic Acids Res. **25:**3389–3402.
2. **Bohmer, M., T. Colby, C. Bohmer, A. Brautigam, J. Schmidt, and M. Bolker.** 2007. Proteomic analysis of dimorphic transition in the phytopathogenic fungus *Ustilago maydis*. Proteomics **7:**675–685.
3. **Bolker, M.** 1998. Sex and crime: heterotrimeric G proteins in fungal mating and pathogenesis. Fungal Genet. Biol. **25:**143–156.
4. **Borkovich, K. A.** 1996. Signal transduction pathways and heterotrimeric G proteins. *In* R. Brambl and G. A. Marzluf (ed.), The mycota. Springer-Verlag, Berlin, Germany.
5. **Cooper, B., W. M. Garrett, and K. B. Campbell.** 2006. Shotgun identification of proteins from uredospores of the bean rust *Uromyces appendiculatus*. Proteomics **6:**2477–2484.
6. **Cousin, A., R. Mehrabi, M. Guilleroux, M. Dufresne, T. Van der Lee, C. Waalwijk, T. Langin, and G. H. J. Kema.** 2006. The MAP kinase-encoding gene *MgFus3* of the nonappressorium phytopathogen *Mycosphaerella graminicola* is required for penetration and in vitro pycnidia formation. Mol. Plant Pathol. **7:**269–278.
7. **Cuomo, C. A., U. Guldener, J. R. Xu, F. Trail, B. G. Turgeon, A. Di Pietro, J. D. Walton, L. J. Ma, S. E. Baker, M. Rep, G. Adam, J. Antoniw, T. Baldwin, S. Calvo, Y. L. Chang, D. Decaprio, L. R. Gale, S. Gnerre, R. S. Goswami, K. Hammond-Kosack, L. J. Harris, K. Hilburn, J. C. Kennell, S.**

Kroken, J. K. Magnuson, G. Mannhaupt, E. Mauceli, H. W. Mewes, R. Mitterbauer, G. Muehlbauer, M. Munsterkotter, D. Nelson, K. O'Donnell, T. Ouellet, W. Qi, H. Quesneville, M. I. Roncero, K. Y. Seong, I. V. Tetko, M. Urban, C. Waalwijk, T. J. Ward, J. Yao, B. W. Birren, and H. C. Kistler. 2007. The *Fusarium graminearum* genome reveals a link between localized polymorphism and pathogen specialization. Science **317:**1400–1402.

8. **Dawe, A. L., G. C. Segers, T. D. Allen, V. C. McMains, and D. L. Nuss.** 2004. Microarray analysis of *Cryphonectria parasitica* Gα- and Gβγ-signalling pathways reveals extensive modulation by hypovirus infection. Microbiology **150:** 4033–4043.
9. **Dean, R. A., N. J. Talbot, D. J. Ebbole, M. L. Farman, T. K. Mitchell, M. J. Orbach, M. Thon, R. Kulkarni, J. R. Xu, H. Pan, N. D. Read, Y. H. Lee, I. Carbone, D. Brown, Y. Y. Oh, N. Donofrio, J. S. Jeong, D. M. Soanes, S. Djonovic, E. Kolomiets, C. Rehmeyer, W. Li, M. Harding, S. Kim, M. H. Lebrun, H. Bohnert, S. Coughlan, J. Butler, S. Calvo, L. J. Ma, R. Nicol, S. Purcell, C. Nusbaum, J. E. Galagan, and B. W. Birren.** 2005. The genome sequence of the rice blast fungus *Magnaporthe grisea*. Nature **434:**980–986.
10. **Douaiher, M. N., P. Halama, and M. C. Janex-Favre.** 2004. The ontogeny of *Stagonospora nodorum* pycnidia in culture. Sydowia **56:**39–50.
11. **Fang, E. G., and R. A. Dean.** 2000. Site-directed mutagenesis of the *magB* gene affects growth and development in *Magnaporthe grisea*. Mol. Plant-Microbe Interact. **13:**1214–1227.
12. **Fernandez-Acero, F. J., I. Jorge, E. Calvo, I. Vallejo, M. Carbu, E. Camafeita, J. A. Lopez, J. M. Cantoral, and J. Jorrin.** 2006. Two-dimensional electrophoresis protein profile of the phytopathogenic fungus *Botrytis cinerea*. Proteomics **6:**S88–S96.
13. **Fessler, M. B., K. C. Malcolm, M. W. Duncan, and G. S. Worthen.** 2002. A genomic and proteomic analysis of activation of the human neutrophil by lipopolysaccharide and its mediation by p38 mitogen-activated protein kinase. J. Biol. Chem. **277:**31291–31302.
14. **Gao, S., and D. L. Nuss.** 1996. Distinct roles for two G protein α subunits in fungal virulence, morphology, and reproduction revealed by targeted gene disruption. Proc. Natl. Acad. Sci. USA **93:**14122–14127.
15. **Giles, N. H., R. F. Geever, D. K. Asch, J. Avalos, and M. E. Case.** 1991. The Wilhelmine E. Key 1989 invitational lecture. Organization and regulation of the *qa* (quinic acid) genes in *Neurospora crassa* and other fungi. J. Hered. **82:**1–7.
16. **Gronover, C. S., D. Kasulke, P. Tudzynski, and B. Tudzynski.** 2001. The role of G protein α subunits in the infection process of the gray mold fungus *Botrytis cinerea*. Mol. Plant-Microbe Interact. **14:**1293–1302.
17. **Gronover, C. S., C. Schorn, and B. Tudzynski.** 2004. Identification of *Botrytis cinerea* genes up-regulated during infection and controlled by the Gα subunit BCG1 using suppression subtractive hybridization (SSH). Mol. Plant-Microbe Interact. **17:**537–546.
18. **Gygi, S. P., Y. Rochon, B. R. Franza, and R. Aebersold.** 1999. Correlation between protein and mRNA abundance in yeast. Mol. Cell. Biol. **19:**1720–1730.
19. **Hane, J. K., R. G. Lowe, P. S. Solomon, K. C. Tan, C. L. Schoch, J. W. Spatafora, P. W. Crous, C. Kodira, B. W. Birren, J. E. Galagan, S. F. Torriani, B. A. McDonald, and R. P. Oliver.** 2007. Dothideomycete plant interactions illuminated by genome sequencing and EST analysis of the wheat pathogen *Stagonospora nodorum*. Plant Cell **19:**3347–3368.
20. **Harwood, C. S., and R. E. Parales.** 1996. The β-ketoadipate pathway and the biology of self-identity. Annu. Rev. Microbiol. **50:**553–590.
21. **Horwitz, B. A., A. Sharon, S. W. Lu, V. Ritter, T. M. Sandrock, O. C. Yoder, and B. G. Turgeon.** 1999. A G protein α subunit from *Cochliobolus heterostrophus* involved in mating and appressorium formation. Fungal Genet. Biol. **26:**19–32.
22. **Jain, S., K. Akiyama, K. Mae, T. Ohguchi, and R. Takata.** 2002. Targeted disruption of a G protein α subunit gene results in reduced pathogenicity in *Fusarium oxysporum*. Curr. Genet. **41:**407–413.
23. **Kaffarnik, F., P. Muller, M. Leibundgut, R. Kahmann, and M. Feldbrugge.** 2003. PKA and MAPK phosphorylation of Prf1 allows promoter discrimination in *Ustilago maydis*. EMBO J. **22:**5817–5826.
24. **Kamper, J., R. Kahmann, M. Bolker, L. J. Ma, T. Brefort, B. J. Saville, F. Banuett, J. W. Kronstad, S. E. Gold, O. Muller, M. H. Perlin, H. A. Wosten, R. de Vries, J. Ruiz-Herrera, C. G. Reynaga-Pena, K. Snetselaar, M. McCann, J. Perez-Martin, M. Feldbrugge, C. W. Basse, G. Steinberg, J. I. Ibeas, W. Holloman, P. Guzman, M. Farman, J. E. Stajich, R. Sentandreu, J. M. Gonzalez-Prieto, J. C. Kennell, L. Molina, J. Schirawski, A. Mendoza-Mendoza, D. Greilinger, K. Munch, N. Rossel, M. Scherer, M. Vranes, O. Ladendorf, V. Vincon, U. Fuchs, B. Sandrock, S. Meng, E. C. Ho, M. J. Cahill, K. J. Boyce, J. Klose, S. J. Klosterman, H. J. Deelstra, L. Ortiz-Castellanos, W. Li, P. Sanchez-Alonso, P. H. Schreier, I. Hauser-Hahn, M. Vaupel, E. Koopmann, G. Friedrich, H. Voss, T. Schluter, J. Margolis, D. Platt, C. Swimmer, A. Gnirke, F. Chen, V. Vysotskaia, G. Mannhaupt, U. Guldener, M. Munsterkotter, D. Haase, M. Oesterheld, H. W. Mewes, E. W. Mauceli, D. DeCaprio, C. M. Wade, J. Butler, S. Young, D. B. Jaffe, S. Calvo, C. Nusbaum, J. Galagan, and B. W. Birren.** 2006. Insights from the genome of the biotrophic fungal plant pathogen *Ustilago maydis*. Nature **444:**97–101.
25. **Kim, S. T., S. Yu, S. G. Kim, H. J. Kim, S. Y. Kang, D. H. Hwang, Y. S. Jang, and K. Y. Kang.** 2004. Proteome analysis of rice blast fungus (*Magnaporthe grisea*) proteome during appressorium formation. Proteomics **4:**3579–3587.
26. **Kozak, M.** 2005. Regulation of translation via mRNA structure in prokaryotes and eukaryotes. Gene **361:**13–37.
27. **Kurose, H.** 2003. $G\alpha_{12}$ and $G\alpha_{13}$ as key regulatory mediator in signal transduction. Life Sci. **74:**155–161.
28. **Lee, N., C. A. D'Souza, and J. W. Kronstad.** 2003. Of smuts, blasts, mildews, and blights: cAMP signaling in phytopathogenic fungi. Annu. Rev. Phytopathol. **41:**399–427.
29. **Le Quere, A., A. Schutzendubel, B. Rajashekar, B. Canback, J. Hedh, S. Erland, T. Johansson, and A. Tunlid.** 2004. Divergence in gene expression related to variation in host specificity of an ectomycorrhizal fungus. Mol. Ecol. **13:**3809–3819.
30. **Lifton, R. P., M. L. Goldberg, R. W. Karp, and D. S. Hogness.** 1978. The organization of the histone genes in *Drosophila melanogaster*: functional and evolutionary implications. Cold Spring Harb. Symp. Quant. Biol. **42:**1047–1051.
31. **Liu, H., A. Suresh, F. S. Willard, D. P. Siderovski, L. Shen, and N. I. Naqvi.** 2007. Rgs1 regulates multiple Gα subunits in *Magnaporthe* pathogenesis, asexual growth and thigmotropism. EMBO J. **26:**690–700.
32. **Liu, S., and R. A. Dean.** 1997. G protein α subunit genes control growth, development, and pathogenicity of *Magnaporthe grisea*. Mol. Plant-Microbe Interact. **10:**1075–1086.
33. **Mann, M., and O. N. Jensen.** 2003. Proteomic analysis of post-translational modifications. Nat. Biotechnol. **21:**255–261.
34. **Marchler-Bauer, A., J. B. Anderson, C. DeWeese-Scott, N. D. Fedorova, L. Y. Geer, S. He, D. I. Hurwitz, J. D. Jackson, A. R. Jacobs, C. J. Lanczycki, C. A. Liebert, C. Liu, T. Madej, G. H. Marchler, R. Mazumder, A. N. Nikolskaya, A. R. Panchenko, B. S. Rao, B. A. Shoemaker, V. Simonyan, J. S. Song, P. A. Thiessen, S. Vasudevan, Y. Wang, R. A. Yamashita, J. J. Yin, and S. H. Bryant.** 2003. CDD: a curated Entrez database of conserved domain alignments. Nucleic Acids Res. **31:**383–387.
35. **Mehrabi, R., and G. H. J. Kema.** 2006. Protein kinase a subunits of the ascomycete pathogen *Mycosphaerella graminicola* regulate asexual fructification, filamentation, melanization and osmosensing. Mol. Plant Pathol. **7:**565–577.
36. **Melin, P., J. Schnurer, and E. G. Wagner.** 2002. Proteome analysis of *Aspergillus nidulans* reveals proteins associated with the response to the antibiotic concanamycin A, produced by *Streptomyces* species. Mol. Genet. Genomics **267:**695–702.
37. **Morel, M., C. Jacob, A. Kohler, T. Johansson, F. Martin, M. Chalot, and A. Brun.** 2005. Identification of genes differentially expressed in extradical mycelium and ectomycorrhizal roots during *Paxillus involutus-Betula pendula* ectomycorrhizal symbiosis. Appl. Environ. Microbiol. **71:**383–391.
38. **Neuhoff, V., N. Arold, D. Taube, and W. Ehrhardt.** 1988. Improved staining of proteins in polyacrylamide gels including isoelectric focusing gels with clear background at nanogram sensitivity using Coomassie brilliant blue G-250 and R-250. Electrophoresis **9:**255–262.
39. **Neves, S. R., P. T. Ram, and R. Iyengar.** 2002. G protein pathways. Science **296:**1636–1639.
40. **Nishimura, M., G. Park, and J. R. Xu.** 2003. The G-beta subunit MGB1 is involved in regulating multiple steps of infection-related morphogenesis in *Magnaporthe grisea*. Mol. Microbiol. **50:**231–243.
41. **Oppermann, U., C. Filling, M. Hult, N. Shafqat, X. Wu, M. Lindh, J. Shafqat, E. Nordling, Y. Kallberg, B. Persson, and H. Jornvall.** 2003. Short-chain dehydrogenases/reductases (SDR): the 2002 update. Chem. Biol. Interact. *143-***144:**247–253.
42. **Paper, J. M., J. S. Scott-Craig, N. D. Adhikari, C. A. Cuomo, and J. D. Walton.** 2007. Comparative proteomics of extracellular proteins in vitro and in planta from the pathogenic fungus *Fusarium graminearum*. Proteomics **7:**3171–3183.
43. **Peter, M., P.-E. Courty, A. Kohler, C. Delaruelle, D. Martin, D. Tagu, P. Frey-Klett, M. Dupleissis, G. Podila, and F. Martin.** 2003. Analysis of expressed sequence tags from the ectomycorhizal basidiomycetes *Lacarria bicolor* and *Pisolithus microcarpus*. New Phytol. **159:**117–129.
44. **Phalip, V., F. Delalande, C. Carapito, F. Goubet, D. Hatsch, E. Leize-Wagner, P. Dupree, A. V. Dorsselaer, and J. M. Jeltsch.** 2005. Diversity of the exoproteome of *Fusarium graminearum* grown on plant cell wall. Curr. Genet. **48:**366–379.
45. **Rampitsch, C., N. V. Bykova, B. McCallum, E. Beimcik, and W. Ens.** 2006. Analysis of the wheat and *Puccinia triticina* (leaf rust) proteomes during a susceptible host-pathogen interaction. Proteomics **6:**1897–1907.
46. **Regenfelder, E., T. Spellig, A. Hartmann, S. Lauenstein, M. Bolker, and R. Kahmann.** 1997. G proteins in *Ustilago maydis*: transmission of multiple signals? EMBO J. **16:**1934–1942.
47. **Richardson, K. C., L. Jarret, and E. H. Finke.** 1960. Embedding in epoxy resins for ultrathin sectioning in electron microscopy. Stain Technol. **35:**313–323.
48. **Sass, J. E.** 1958. Botanical microtechnique. Iowa State University Press, Ames, IA.
49. **Sexton, A. C., and B. J. Howlett.** 2001. Green fluorescent protein as a

reporter in the Brassica-*Leptosphaeria maculans* interaction. Physiol. Mol. Plant Pathol. **58:**13–21.
50. **Siewers, V., M. Viaud, D. Jimenez-Teja, I. G. Collado, C. S. Gronover, J. M. Pradier, B. Tudzynski, and P. Tudzynski.** 2005. Functional analysis of the cytochrome P450 monooxygenase gene *bcbot1* of *Botrytis cinerea* indicates that botrydial is a strain-specific virulence factor. Mol. Plant-Microbe Interact. **18:**602–612.
51. **Simon, M. I., M. P. Strathmann, and N. Gautam.** 1991. Diversity of G proteins in signal transduction. Science **252:**802–808.
52. **Smale, S. T., and J. T. Kadonaga.** 2003. The RNA polymerase II core promoter. Annu. Rev. Biochem. **72:**449–479.
53. **Solomon, P. S., R. G. T. Lowe, K.-C. Tan, O. D. C. Waters, and R. P. Oliver.** 2006. *Stagonospora nodorum*: cause of stagonospora nodorum blotch of wheat. Mol. Plant Pathol. **7:**147–156.
54. **Solomon, P. S., K. Rybak, R. D. Trengove, and R. P. Oliver.** 2006. Investigating the role of calcium/calmodulin-dependent protein signalling in *Stagonospora nodorum*. Mol. Microbiol. **62:**367–381.
55. **Solomon, P. S., K.-C. Tan, and R. P. Oliver.** 2005. Mannitol 1-phosphate metabolism is required for sporulation in planta of the wheat pathogen *Stagonospora nodorum*. Mol. Plant-Microbe Interact. **18:**110–115.
56. **Solomon, P. S., K.-C. Tan, P. Sanchez, R. M. Cooper, and R. P. Oliver.** 2004. The disruption of a Gα subunit sheds new light on the pathogenicity of *Stagonospora nodorum* on wheat. Mol. Plant-Microbe Interact. **17:**456–466.
57. **Solomon, P. S., S. W. Thomas, P. Spanu, and R. P. Oliver.** 2003. The utilisation of di/tripeptides by *Stagonospora nodorum* is dispensable for wheat infection. Physiol. Mol. Plant Pathol. **63:**191–199.
58. **Solomon, P. S., O. D. Waters, C. I. Jorgens, R. G. Lowe, J. Rechberger, R. D. Trengove, and R. P. Oliver.** 2006. Mannitol is required for asexual sporulation in the wheat pathogen *Stagonospora nodorum* (glume blotch). Biochem. J. **399:**231–239.
59. **Solomon, P. S., O. D. Waters, J. Simmonds, R. M. Cooper, and R. P. Oliver.** 2005. The *Mak2* MAP kinase signal transduction pathway is required for pathogenicity in *Stagonospora nodorum*. Curr. Genet. **48:**60–68.
60. **Solomon, P. S., O. D. C. Waters, and R. P. Oliver.** 2007. Decoding the enigmatic mannitol in filamentous fungi. Trends Microbiol. **15:**257–262.
61. **Solomon, P. S., T. J. G. Wilson, K. Rybak, K. Parker, R. G. T. Lowe, and R. P. Oliver.** 2006. Structural characterisation of the interaction between *Triticum aestivum* and the dothideomycete pathogen *Stagonospora nodorum*. Eur. J. Plant Pathol. **114:**275–282.
62. **Spurr, A. R.** 1969. A low-viscosity epoxy resin embedding medium for electron microscopy. J. Ultrastruct. Res. **26:**31–43.
63. **Taylor, N. L., J. L. Heazlewood, D. A. Day, and A. H. Millar.** 2005. Differential impact of environmental stresses on the pea mitochondrial proteome. Mol. Cell. Proteomics **4:**1122–1133.
64. **Teichert, S., B. Schonig, S. Richter, and B. Tudzynski.** 2004. Deletion of the *Gibberella fujikuroi* glutamine synthetase gene has significant impact on transcriptional control of primary and secondary metabolism. Mol. Microbiol. **53:**1661–1675.
65. **Venable, J. H., and R. Coggshall.** 1965. A simplified lead citrate stain for electron microscopy. J. Cell Biol. **25:**407–408.
66. **Yamagishi, D., H. Otani, and M. Kodama.** 2006. G protein signaling mediates developmental processes and pathogenesis of *Alternaria alternata*. Mol. Plant-Microbe Interact. **19:**1280–1288.